Desantes Fernández, JM.; García Oliver, JM.; Pastor Enguídanos, JM.; Pandal-Blanco, A. (2016). Coupled/decoupled spray simulation comparison of the ECN spray a condition with the Sigma-Y Eulerian atomization model. International Journal of Multiphase Flow. 80:89-99. doi:10.1016/j.ijmultiphaseflow.2015.12.002.

Coupled / Decoupled Spray Simulation Comparison of the ECN spray A Condition with the $\mathbf{\Sigma}$-Y Eulerian Atomization Model

J.M. Desantes[a], J.M. García-Oliver[a], J.M. Pastor[a], A. Pandal[a,*], E. Baldwin[b], D.P. Schmidt[b]

[a] *CMT-Motores Térmicos, Universitat Politècnica de València, Spain*
[b] *Department of Mechanical and Industrial Engineering, University of Massachusetts, Amherst, USA*

Abstract

This work evaluates the performance of the Σ-Y Eulerian atomization model at reproducing the internal structure of a diesel spray in the near-field. In the study, three different computational domains have been used in order to perform 3D and 2D coupled simulations, where the internal nozzle flow and external spray are modeled in one continuous domain, and 2D decoupled simulations, where only the external spray is modeled. While the 3D simulation did the best job of capturing the dense zone of the spray, the 2D simulations also performed well, with the coupled 2D simulation slightly outperforming the decoupled simulation. The similarity in results between the coupled and the decoupled simulation show that internal and external flow calculations can be performed independently. In addition, the use of spatially averaged nozzle outlet conditions, in the case of an axisymmetric (single-hole) convergent nozzle, leads to a slightly worse near-field spray predictions but to an accurate far-field ones. Finally, a novel constraint on turbulent driven mixing multiphase flows is introduced which prevents the slip velocity from exceeding the magnitude of the turbulent fluctuations through a realizable Schmidt number. This constraint increased model stability, allowing for a 4x increase in Courant number.

Keywords: Eulerian, Diesel, Coupled simulation, Near-field, CFD,

*Corresponding author
Email address: adpanbla@mot.upv.es (A. Pandal)

1. Introduction

In recent years, increasing concern for the environment has lead to more restrictive regulations on diesel engine emissions all over the world. In addition to this, the cost of diesel fuel is high and is expected to increase in the future. For these reasons, it is necessary to achieve both high efficiency and reduced emissions in modern diesel engines. Many of the improvements to be made to accomplish this goal are related to the fuel injection process and the subsequent fuel-air mixing process. This is because these processes play a major role in combustion and pollutant formation [10, 27, 28]. Therefore, an accurate prediction of these processes is required in order to produce reliable engine performance and emissions predictions.

Diesel spray modeling has been carried out by means of the Discrete Droplet Method (DDM) [12] for more than 30 years. Although commonly used [1, 21, 22, 45], it presents some well known drawbacks for dense two-phase flow simulations. For example, this method is best suited for low liquid volume fraction flows and it often assumes homogeneously distributed parcels in the computational cells. These conditions are not present in the near nozzle flow of diesel sprays. Lagrangian particle tracking approach fails in this region, because nearly all existing drag, collision, breakup, and vaporization models are based on assumptions of near-spherical droplets in a sparse spray. However, the Σ-Y atomization model [39] has emerged for diesel spray simulations [9, 11, 16, 20, 26] as a promising alternative to classical Lagrangian models. In this kind of model, an Eulerian description is applied to solve the two-phase flow together with an interface surface density equation to compute the extent of the atomization process. In order to model the spray downstream dilute regions, the Σ-Y model could include a transition to Lagrangian description, the so-called ELSA model [4, 20], but also fully-eulerian approaches has shown successful predictions in this region[3, 16]. This model emphasizes the turbulent mixing of the gas and liquid, which is consistent with the observations of Siebers [33, 34, 35], based on numerous experiments, that 'the processes of atomization and the ensuing interphase transport of mass and energy at droplet surfaces are not limiting steps with respect to fuel vaporization in DI diesel sprays'. A more recent work [6] indicates that the in-cylinder conditions for diesel fuel injection are supercritical or near-supercritical. Under these conditions, the gas/liquid interface disappears and

spray simulation becomes entirely an exercise in modeling turbulent mixing. As a result, fully Eulerian treatments of the dense spray region seem to have both numerical and physical advantages. Additionally, an extensive comparison between traditional Lagrangian-DDM models and this Eulerian Σ-Y model was made at the Engine Combustion Network 2nd Workshop (ECN2) [13], showing that the model used in this work delivered the most accurate predictions. More benefits of the Eulerian approach can also be found in [9, 43, 44].

As it is known, nozzle geometric parameters have a great influence on the spray behavior [27, 28]. Thus, including nozzle effects by coupling internal and external flow simulations leads to a better representation of reality. These simulations are usually done by a two-step methodology [3, 36, 37], transferring all the spatial and temporal fields from an internal flow simulation to a primary break-up (blob) model, which uses them to initialize droplet properties for the Lagrangian external spray simulation. This coupling methodology presents several issues derived from the mapping procedure because of the different computational time steps required by the two simulations. Additionally, this methodology needs to use phenomenological models to capture the influence of in-nozzle flow and fuel properties on spray [36, 37]. Alternatively, these issues can be avoided by using an eulerian atomization model to simulate internal and external flow together in one simulation [32, 43, 44]. This is a natural approach for including nozzle geometry flow effects on spray calculations [26] and it provides a more suitable description for the primary atomization occurring in the near-field of diesel sprays [4]. However, 3D modeling of internal and external flow together in an Eulerian framework can be computationally expensive, specially if downstream spray regions are included [43, 44]. Because of that, it seems interesting to investigate the potential suitability of eulerian decoupled simulations [3, 41].

In the present work, a fully Eulerian Σ-Y model [16], implemented in the OpenFOAM CFD open source c++ library [42], is evaluated to simulate coupled/decoupled nozzle flow simulations against experimental measurements available from the database of the Engine Combustion Network [14]. In order to conduct this study, some of the conclusions presented by [32] will be used as initial set-up. The aim of the paper is to evaluate the capabilities of the Σ-Y Eulerian model to reproduce the internal structure of a diesel spray in the near-field. The study investigates the implications of the coupled internal/external flow simulations, the effectiveness of 2D simulations in comparison to 3D and the accuracy that can be achieved by different decou-

pled simulations. In addition to this, a novel constraint on turbulent mixing is derived and implemented.

2. Σ-Y model description

The Σ-Y model considers the liquid/gas mixture as a pseudo-fluid with a single velocity field. Under the assumption that the flow exiting the injector is operating at large Reynolds and Weber numbers, it is possible to assume a separation of the large scale flow features, such as mass transport, from the atomization process occurring at smaller scales. This allows the direct simulation of the large scale bulk transport of the liquid while unresolved turbulent transport is modeled using standard closures such as those used in Reynolds-averaged turbulence models.

To track the dispersion of the liquid phase an indicator function is used, taking a value of unity in the liquid phase and zero in the gas phase. The mean liquid volume fraction is denoted ($\overline{Y}$) and the mean mass averaged fraction is defined as ($\tilde{Y} = \frac{\overline{\rho Y}}{\bar{\rho}}$). Favre averaging the transport equation for the liquid mass fraction yields Eq. (1)

$$\frac{\partial \bar{\rho}\tilde{Y}}{\partial t} + \frac{\partial \bar{\rho}\tilde{u}_i\tilde{Y}}{\partial x_i} = -\frac{\partial \bar{\rho}\widetilde{u'_i Y'}}{\partial x_i} \tag{1}$$

where u' denotes the density weighted turbulent fluctuations in velocity and Y' denotes turbulent fluctuations in liquid mass fraction. The turbulent diffusion liquid flux term, $\widetilde{u'_i Y'}$, captures the effect of the relative velocity between the two phases [40]. This term is modeled using a standard turbulent gradient flux model, which law successfully worked for Diesel spray compared to DNS results, as indicated in [8].

$$\bar{\rho}\widetilde{u'_i Y'} = -\frac{\mu_t}{Sc}\frac{\partial \tilde{Y}}{\partial x_i} \tag{2}$$

where μ_t is the turbulent viscosity and Sc is the constrained Schmidt number which will be described later in this section.

While the approach used here assumes that the resolved momentum of the liquid/gas mixture can be characterized by a single bulk velocity, the slip velocity can be expressed explicitly as derived by [7] and seen in Eq. (3).

$$u_i|_l - u_i|_g = \frac{1}{\tilde{Y}\left(1-\tilde{Y}\right)} \cdot \widetilde{u'_i Y'} \tag{3}$$

Under the assumption that the two phases form an immiscible mixture, the mass-averaged value of the indicator function is related to the density by:

$$\frac{1}{\bar{\rho}} = \frac{\tilde{Y}}{\rho_l} + \frac{1-\tilde{Y}}{\rho_g} \tag{4}$$

An equation of state is then assigned to each phase. The gas phase obeys an ideal gas law, while the liquid phase is estimated following the Hankinson-Brobst-Thomson (HBT) correlation [31], in which the liquid density is a function of temperature (T) and pressure (p).

To close the above system of equations, the temperature is obtained from a bulk mixture enthalpy equation expressed in the following terms:

$$h\left(T\right) = \tilde{Y} \cdot h_l\left(T\right) + \left(1-\tilde{Y}\right) \cdot h_g\left(T\right) \tag{5}$$

Here h_l and h_g denote the enthalpy of the liquid and gas phases respectively, and are calculated as the integrals of

$$dh_l = c_{p,l} dT + \left(1-\alpha T\right)\frac{dp}{\rho} \tag{6}$$

$$dh_g = c_{p,g} dT \tag{7}$$

where $c_{p,i}$ is the specific heat capacity at constant pressure. This is obtained as a function of temperature T from a set of coefficients taken from JANAF tables of thermodynamics. For the liquid phase, then it is applied the Rowlinson-Bondi equation [31]. The coefficient of thermal expansion, α, is a function of pressure and temperature and it is calculated through its definition [5], as explained in [24].

Finally, being h the static enthalpy implemented through the following conservation equation, where α_{eff} is the effective turbulent thermal diffusivity and $\tau_{ij}\frac{\partial u_j}{\partial x_i}$ the viscous dissipation:

$$\frac{\partial \bar{\rho} h}{\partial t} + \frac{\partial \bar{\rho} \tilde{u}_i h}{\partial x_i} - \frac{\partial}{\partial x_i}\left(\alpha_{eff}\frac{\partial h}{\partial x_i}\right) = \frac{\partial p}{\partial t} + u_i\frac{\partial p}{\partial x_i} + \tau_{ij}\frac{\partial u_j}{\partial x_i} \tag{8}$$

The solution of the above equations fully characterizes the large-scale bulk motion of the flow. Several other options exist for obtaining closure in the above system of equations (see for example the discussion in [7] and [38]).

Conversely, the small scale atomization is modeled by solving a transport equation for the evolution of the density of interphase surface area Σ, originally proposed by [39]. The evolution equation is given by

$$\frac{\partial \overline{\Sigma}}{\partial t} + \frac{\partial \tilde{u}_j \overline{\Sigma}}{\partial x_j} = \frac{\partial}{\partial x_j}\left(D_\Sigma \frac{\partial \overline{\Sigma}}{\partial x_j}\right) + (A + a)\,\overline{\Sigma} - V_s \overline{\Sigma}^2 \tag{9}$$

A detailed explanation of the different terms in Eq. (9) and how relevant quantities for spray characterisation, such as Sauter Mean Diameter (SMD), are obtained together with further description of the numerical implementation of this solver can be found in [16]. Although in the present work no comparison of SMD has been made due to the absence of such measurements in the investigated cases, detailed comparisons in the literature indicate that this equation provides good trends in terms of SMD predictions [3, 16, 40, 41] as well as when comparing to DNS results [8, 20].

2.1. A Realizable Constraint to Turbulent Mixing

When an intact liquid jet first contacts gas near the nozzle exit, the gradient of the mass fraction (Y) is nearly infinite. With the standard turbulent gradient flux model, this can produce unbounded, unrealistic mixing velocities. This unbounded mixing may have only modest impacts on overall model accuracy, but it causes local errors that have significant stability implications. For this reason, a constraint on the mixing velocity has been implemented in this study.

For multiphase flows with turbulent driven mixing, it is logical that the slip velocity should not exceed the magnitude of the turbulent velocity fluctuations,

$$u_i|_l - u_i|_g \leq u'_i \tag{10}$$

Using the expression for slip velocity, Eq. (3), with the definition of turbulent kinetic energy for isotropic turbulence, the following constraint is derived,

$$\frac{1}{\tilde{Y}\left(1-\tilde{Y}\right)} \cdot \widetilde{u'_i Y'} \leq \sqrt{\frac{2}{3}k} \tag{11}$$

This can then be imposed on the turbulent diffusion liquid flux term by combining Eq. (11) and Eq. (2). The result yields a lower bound to the Schmidt number which can been seen below in Eq. (12).

$$Sc \geq \frac{\mu_t}{\bar{\rho}\sqrt{2/3k}\tilde{Y}(1-\tilde{Y})}\frac{\partial \tilde{Y}}{\partial x_i} \tag{12}$$

Table 1: Conditions for non-evaporating Spray A experiment

Fuel	n-Dodecane
Ambient composition	100% N2
Injection pressure [MPa]	150
Ambient temperature [K]	303
Ambient density [kg/m^3]	22.8
Fuel injection temperature [K]	343

Note here that the value of the slip velocity ($\sqrt{2/3k}\tilde{Y}(1-\tilde{Y})$) is bounded to a positive value (always greater than $1e^{-6}$ m/s) to avoid the denominator to be zero near the orifice exit ($\tilde{Y} \approx 1$). The implementation is then achieved by making the Schmidt number in Eq. (2) a field and setting its value to whichever is greater, the lower bound prescribed by Eq. (12) or the conventional Schmidt number of 0.9 [16].

3. Experimental data

In order to evaluate and validate the model applied to coupled nozzle flow and spray simulations, the ECN Spray A database [14, 17] has been used. The "Spray A" condition consists of a free diesel spray injected into a quiescent environment, where well-defined boundary conditions and experimental data are available for model validation purposes. The nominal condition for Spray A corresponds to 150 MPa injection pressure, 900 K ambient temperature and 22.8 kg/m^3 as ambient density.

In this case, the Spray A non-evaporating condition of ECN is used in order to evaluate the model in terms of the near-field structure (dense region) of diesel sprays, taking advantage of the valuable x-ray radiography measurements available at ECN database. This experiment is conducted with the ambient gas at room temperature (303 K) due to the x-ray transparent polymer windows used, which cannot be used at high temperature. Nevertheless, the same ambient density of the nominal evaporating Spray A condition is matched in order to reproduce similar conditions for the spray breakup process, assuming that density is a more critical parameter than pressure for atomization [25]. The main conditions of this experiment are presented in Table 1. Further details about the experimental set-up are provided in [19].

Table 2: Nozzle geometric characteristics for single-hole Spray A ECN injector

Injector Serial#	$D_o[\mu m]$	$D_i[\mu m]$	L/D_o[-]	r/D_o[-]	k-factor	exit offset [μm]
210675	89.4	116	11.5	0.23	2.7	53

Detailed internal nozzle geometric characterization has been performed for the injector employed in these experiments, where the main characteristics are presented in Table 2. D_o, D_i, L and r denote nozzle orifice outlet diameter, nozzle orifice inlet diameter, length, and inlet radius, respectively. The nozzle convergence is described by the k-factor, as defined in [23].

4. Computational Domain and Model set-up

The single-hole Spray A injector (Serial# 210675) presents a particularity in form of an offset of the orifice outlet with respect to the needle axis. Thus a full three-dimensional domain is needed for performing the CFD simulations, as depicted in Fig. 1. This computational domain includes a cylindrical spray chamber 12 mm in length and 14 mm in diameter. In Fig. 1, the mesh structure can also be seen. It consists of 2.25 million hexahedral cells with a minimum cell size of 1.5 μm near the walls inside the nozzle and a maximum cell size of 250 μm far from the orifice exit.

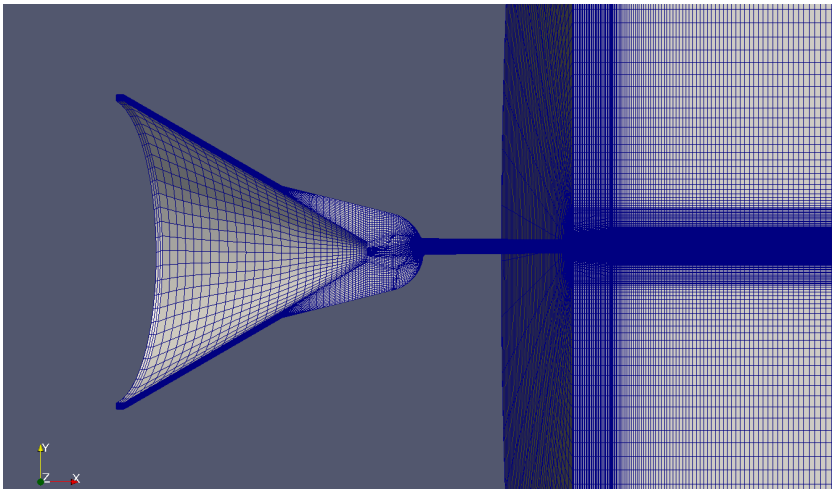

Figure 1: Computational grid for three-dimensional Spray A simulations

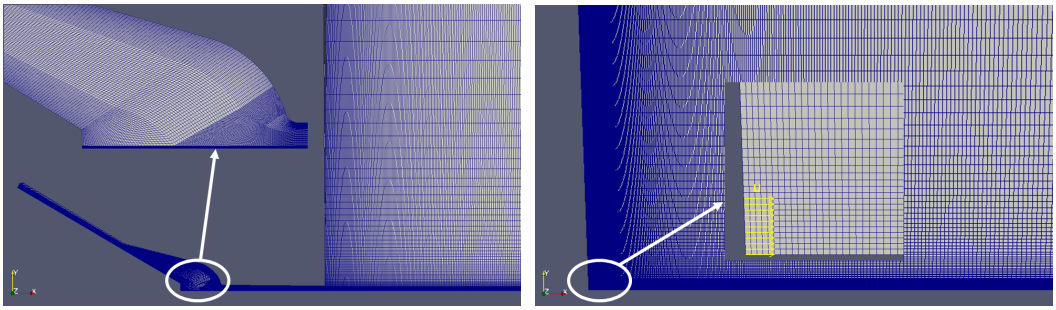

(a) Grid used for coupled nozzle-spray simulations

(b) Grid used for de-coupled spray simulations

Figure 2: Computational grids for two-dimensional Spray A simulations

In addition to the three-dimensional mesh, a two-dimensional axisymmetric one is used in order to reduce the computational cost. The geometry dimensions are the same as in the 3D domain as well as the same order mesh resolution, see Fig. 2a. The mesh is structured with non-uniform grid resolution. There are 89000 cells with 72 elements at the orifice exit. This mesh was built following the results of a sensitivity study previously performed as indicated in [24, 32].

Finally, in order to simulate a fully developed spray with the Σ-Y Eulerian model, a 2D axisymmetric computational domain without the nozzle geometry is considered. The mesh is structured with non-uniform grid resolution. There are 20 cells along the orifice diameter, keeping an aspect ratio close to one in the near nozzle region, as depicted in Fig. 2b. The non-uniform grid resolution consists of cells with an expansion ratio of 1.01 and 1.06 in the axial and radial directions, respectively, as indicated in [16]. Note that all the computational domains use the axis orientation convention from Kastengren et al. [17].

Boundary conditions selected for all the walls of the domains are no-slip. A non-reflexive boundary condition is used for the outlet and a time varying velocity condition is used for the inlet. The inlet velocity is obtained from experimental mass flow measurements, domain inlet area and fuel density. A uniform velocity distribution at the domain inlet is assumed. This inlet condition was used instead of a constant pressure profile because a constant pressure profile would not capture the experimentally observed time oscillations in the flow. This is because these oscillations are highly influenced by

Table 3: Computational grid cases and Set-Up

Case#	Computational mesh	BC inlet set-up
1	3D internal-external geometry	velocity profile from mass flow rate
2	2D internal-external geometry	velocity profile from mass flow rate
3	2D external geometry	simulated fields at nozzle exit of case 2
4	2D external geometry	uniform top-hat profile

the transient needle movement profile, and these simulations used a static mesh with the needle positioned at maximum lift.

The k-ϵ turbulence model was set to perform the simulations. Due to the well known round jet spreading overprediction of k-ϵ type models [30], a corrected value (1.60) for $C_{1\epsilon}$ is used, as indicated in [16]. Pope [30] has previously suggested that the latter value should be used for round jets. The liquid turbulent flux closure [2] is calculated by means of a gradient closure, the discretization of the divergence terms was solved with a Gamma NVD scheme, and a first order Euler scheme is applied for time derivative terms. Note that x-ray measurements deliver ensemble-averaged values from 128 to 256 individual spray events. Thus, RANS can be considered a reasonable modeling approach, which can be validated by comparing to such measurements.

In Table 3, the four different cases simulated are summarized, including the type of computational domain and the boundary conditions set-up employed.

5. Results and Discussion

5.1. Realizable Schmidt Number Evaluation

An evaluation of the realizable Schmidt number was conducted with 2D coupled simulations. Two cases were run, one with a constant Schmidt number of 0.9 and one with the realizable expression described in sec. 2.1. In Fig. 3, a snapshot of the distribution of realizable Schmidt number, together with a 90% liquid contour volume fraction is shown to help understand where this constraint is effectively acting. This constraint arises from physical phenomena, i.e., slip velocity should not exceed the magnitude of turbulent

fluctuations. When using a gradient closure for liquid turbulent flux, the proposed constraint limits unrealistic and unbounded turbulent mixing velocities, thus it improves both physics description and numerical stability. It can be observed that the constraint takes effect within the intact core of the liquid fuel (Liquid Volume Fraction > 0.9), where the unrealistic mixing velocities (numerically introduced) may appear.

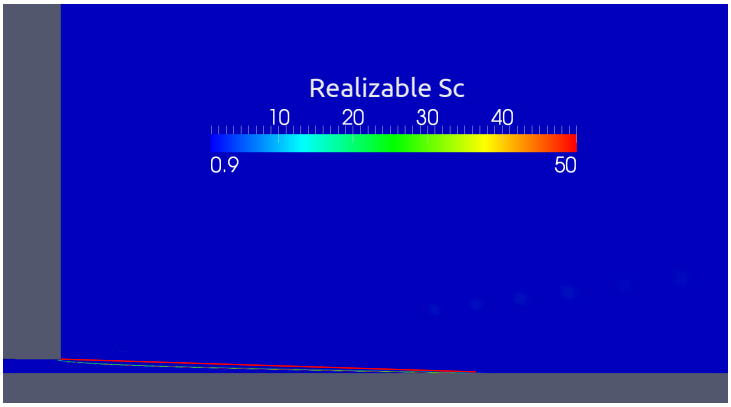

Figure 3: Computed CFD field of the realizable Schmidt number [-] and contour of 90 % Liquid Volume Fraction (red solid line) at 500 μs after SOI.

In Fig. 4, the model predicted results of projected mass density are compared against x-ray radiography measurements conducted at Argonne National Laboratory. The variable used for comparison is the projected mass density of the fuel, which is calculated by a line-of-sight integration along the x-ray beam [19, 29]. A similar procedure is replicated with the data from simulations to enable fair comparisons against experiments. This comparison is made at 0.1 mm, 2 mm, and 6 mm downstream of the nozzle exit. The results are not dramatically different and only at 0.1 mm can some insignificant differences be noticed.

Another useful quantity obtained from the x-ray radiography measurements is the transverse integrated mass (TIM), which is obtained from the integral of the projected density across the transverse position at a particular axial location [18]. In Fig. 5, it is shown that the constrained case has a slightly lower TIM value right at the nozzle exit and again in the far field, due to the limited liquid mass diffusion. It has to be noticed that TIM is related to spray dispersion,i.e., higher TIM indicates that spray mixing is faster.

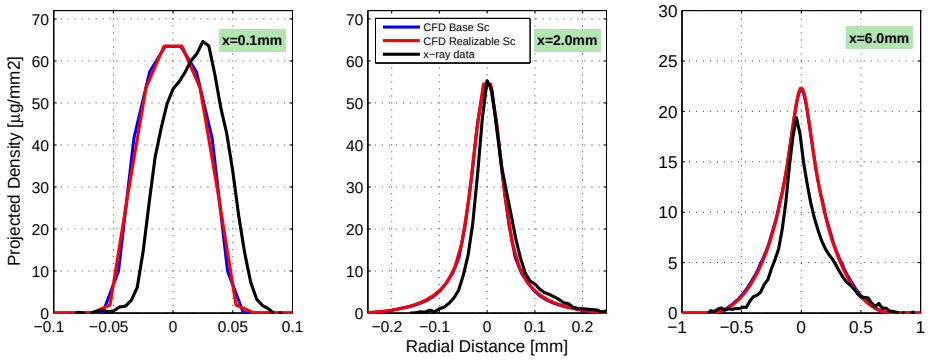

Figure 4: Computed and measured profiles of projected mass density [μg/mm^2] at 500 μs after SOI at axial locations of 0.1 mm, 2 mm, and 6 mm downstream of the nozzle exit

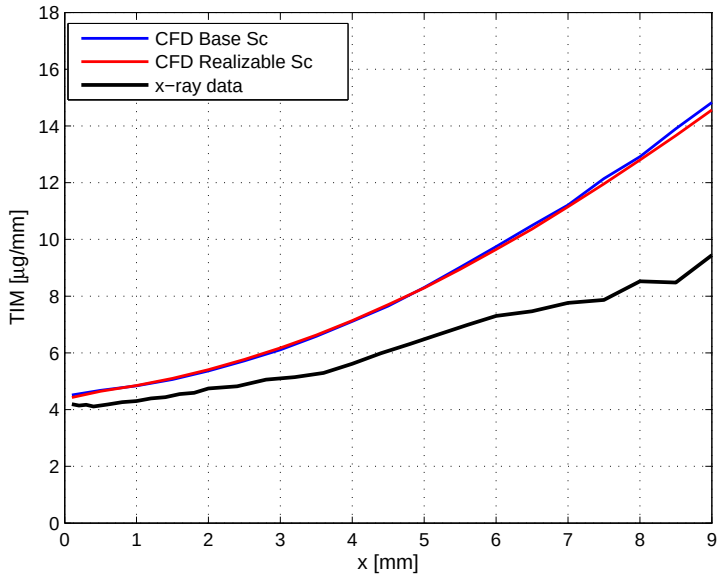

Figure 5: Computed and measured transverse integrated mass (TIM) along the axis at 500 μs after SOI

Overall, a reasonable agreement with experimental data is provided and the tendencies are well captured, independently of which Schmidt number is used. No great differences could be detected between the predicted values of the simulations, as can be seen in the projected density profiles as well

Table 4: Computational cost comparison between 3D and 2D simulations

Type of simulation	Wall Clock Time (hours)	Number of CPU
3D	936	24
2D	72	12

as the TIM within the near-nozzle region. The remarkable utility of this constrained formulation is that it improves the numerical stability, allowing the simulation to run with a Courant number four times greater than the reference case. As a result, the following simulations have been made using this constrained Schmidt number formulation.

5.2. 3D vs 2D Coupled Simulations

The next study conducted was a comparison of the coupled 3D and 2D simulations to the experimental data. Obviously, only the 3D geometry is capable of capturing the experimental asymmetries. However, investigating the effectiveness of 2D simulations is of interest because of the benefit of reduced computational cost, see Table 4.

From the projected density contours, Fig. 6, it is seen that the simulations can capture the fuel distribution in the very near nozzle region (i.e., within 6 mm) with both meshes. Downstream of this axial position, the radial dispersion of simulations tend to be over-predicted, as also seen in Fig. 5. Both grids report almost the same results, so a more detailed comparison should be made.

The projected density along the transverse direction comparing the simulations and x-ray radiography data is shown at 0.1 mm, 2 mm, and 6 mm downstream of the nozzle exit in Fig. 7. The 3D computational profiles shown in this figure were made along the transverse directions Y and Z, respectively. The profiles in both 3D directions are essentially identical; however, the profile which corresponds to the Y axis is shifted due to the off-center nozzle position. At the three axial positions, a very similar projected density profile is predicted by the model independent of the used grid. Comparing the CFD predictions with the experimental measurements, the largest differences can be observed at 6 mm. Here projected density is well matched in terms of radial dispersion but over-predicted in terms of peak value.

As explained in [43], the mass distribution data can be used to describe the trends in the axial spray velocity under steady-state conditions. This

is done by means of the TIM, which is inversely proportional to the mass-averaged axial spray velocity at any given axial location. Thus, the relative velocity can be obtained by normalizing the TIM at any location with the TIM at the nozzle exit. This is used to compare the axial spray velocity profile along the axis among the simulations and x-ray data. Fig. 8 shows the predicted results of simulations, using the two different computational domains, compared with measurements. The relative velocity profiles for both 2D and 3D computations are essentially identical, which shows that 2D simulations are adequate if nozzle asymmetry does not need to be captured. Compared with the experimental profile, the relative velocity is increasingly under-predicted with axial position, with a noticeable divergence occurring at 3 mm and 6 mm. This is indicative, accordingly with previous comments,

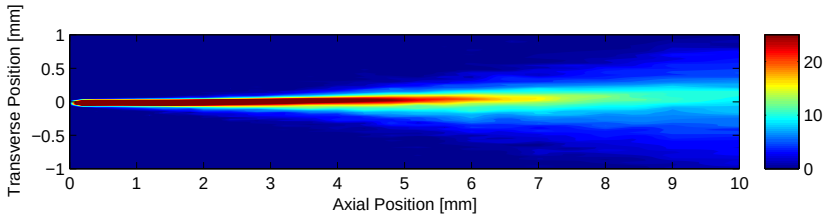

(a) x-ray data

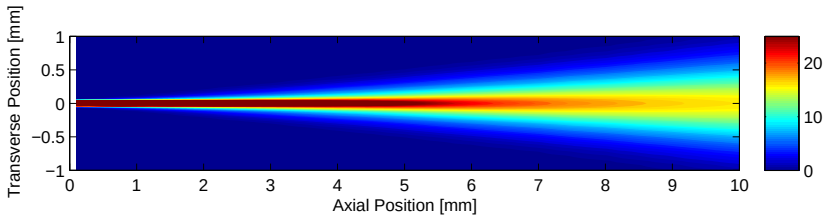

(b) 2D baseline CFD simulation

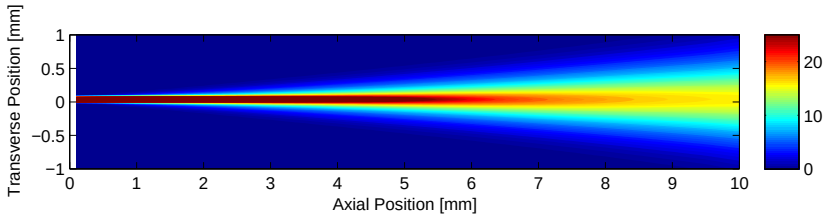

(c) 3D baseline CFD simulation

Figure 6: Projected mass density distributions [μg/mm^2] at 500 μs after SOI from x-ray data and baseline CFD simulations

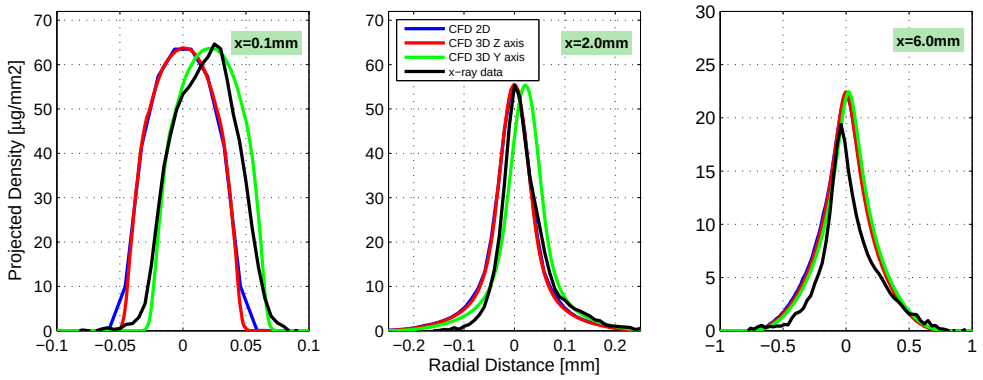

Figure 7: Computed and measured profiles of projected mass density [μg/mm^2] at 500 μs after SOI at axial locations of 0.1 mm, 2 mm, and 6 mm downstream of the nozzle exit

that simulations predicts enhanced spray mixing compared to the results derived from measurements, as also obtained by [43].

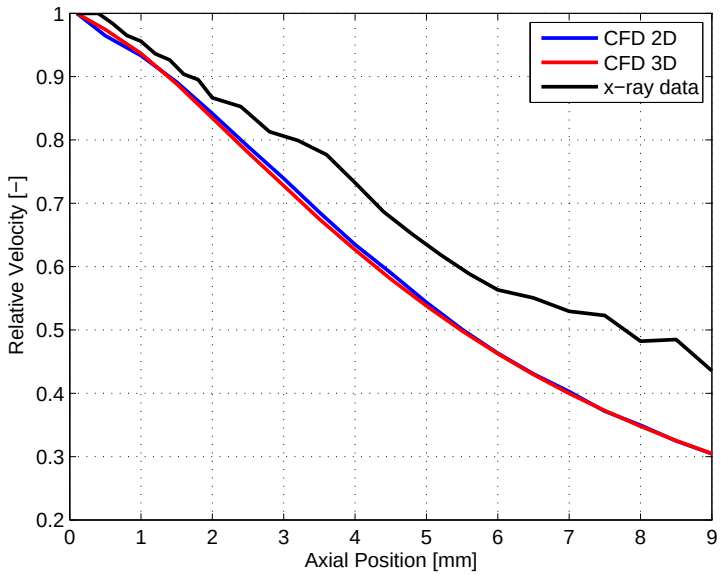

Figure 8: Computed and measured mass-average spray velocity along the axis at 500 μs after SOI

Overall, the Σ-Y model provides good agreement with experimental data

and can capture the trend of the internal structure of a diesel spray fairly well in the near-field. This is shown in the projected density profiles as well the relative velocity profiles. Beyond 6 mm downstream of the nozzle exit, the peak projected mass density is over-predicted. Furthermore, it is clear that the 2D axisymmetric domain is completely capable of predicting satisfactory results when asymmetry is not present at the nozzle.

5.3. 2D Decoupled Simulations

To conclude the evaluation of the Σ-Y Eulerian model, two more simulations have been made using the 2D axisymmetric computational domain without the nozzle geometry. The first simulation was conducted using as an inlet boundary condition the fields obtained at the nozzle exit in the 2D coupled simulation. To do that, the mapped boundary condition of OpenFOAM is used. The other simulation was made using as an inlet boundary condition a top-hat (TH) radial profile of axial velocity obtained from mass flow rate and momentum flux measurements [27]. In this case, the turbulent intensity and the length scale were taken as area-averaged values at nozzle exit from coupled simulation.

Here, the analysis is started with the projected density along the transverse direction comparing the simulations and x-ray radiography data at 0.1 mm, 2 mm, and 6 mm downstream of the nozzle exit in Fig. 9. This figure shows the profiles of the 2D coupled simulation (as reference) against the profiles achieved with the decoupled ones. First, it has to be highlighted that the radial dispersion of all profiles is quite similar, only at the first axial location is the coupled simulation slightly narrower. More differences appear when comparing peak projected density. At the three locations, the profiles predicted with the flat inlet velocity profile achieved a slightly worse value, being at 6 mm downstream the one which diverges more from the experimental measurements.

In Fig. 10 the relative velocity axial profile as derived from TIM is shown. Once again, the three profiles are quite similar and the trends are well captured. The coupled simulation achieved the best match with the experimental measurements and predicted a less diffusive spray as indicated by slower relative velocity decay.

In addition, it is interesting to study the influence of the internal flow simulation on typical global spray parameters such as penetration and also on the liquid volume fraction (LVF) field, to see effects on the spray tip penetration evolution, spray dispersion and the intact core length. Consequently,

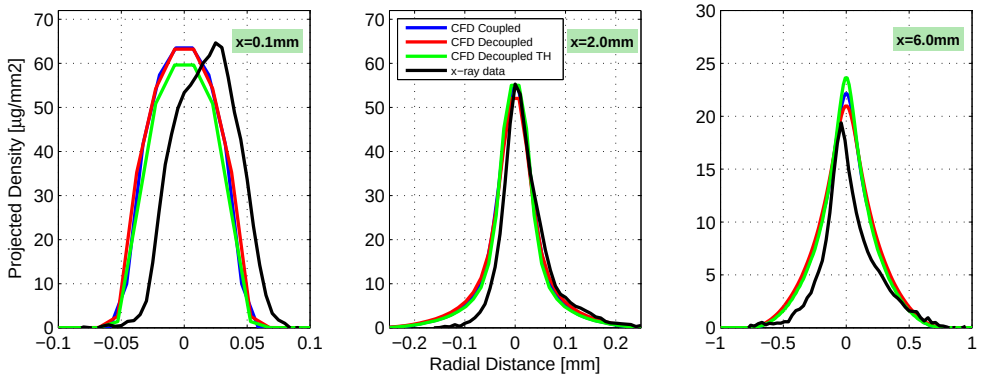

Figure 9: Computed and measured profiles of projected mass density [μg/mm^2] at 500 μs after SOI at axial locations of 0.1 mm, 2 mm, and 6 mm downstream of the nozzle exit for different types of 2D simulations

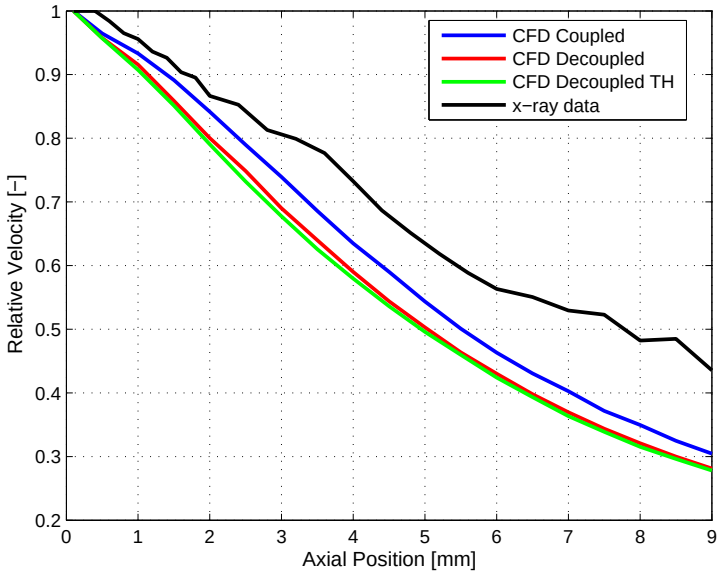

Figure 10: Computed and measured mass-average spray velocity along the axis at 500 μs after SOI for different types of 2D simulations

the simulations conducted using the mesh without the internal nozzle geometry (because of computational costs) have been run to a time of 3 ms after start of injection. In Fig. 11 spray penetration (left) and predicted centerline liquid volume fraction profiles (right) are compared. In terms of spray pene-

tration, some impact in the first 0.5 ms can be observed, being the decoupled simulation the only one that is capable of matching the experimental measurements. Then both simulated curves tend to the same values. In terms of profiles of liquid volume fraction on the axis, it must be noted that experimental measurements are available only within the first 12 mm. This measurements, available at [15], are made by a tomography reconstruction of radiography data for liquid volume fraction [29]. The decoupled simulation, with the nozzle profile derived from the coupled calculations, clearly performs better being able to match exactly the decay of the liquid volume fraction and predicting an intact liquid core ($LVF > 0.9$) almost in the range estimated by recent analyses in [29]. The differences in near-nozzle liquid volume profiles should be caused by using top-hat nozzle outlet profiles instead of those from coupled nozzle internal and external flow calculations.

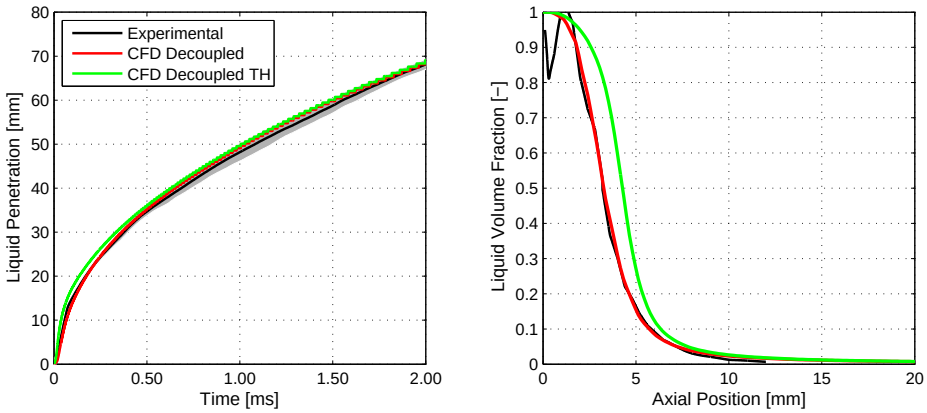

Figure 11: Spray penetration [left] and computed centerline liquid volume fraction at 1 ms after SOI [right] for different types of 2D decoupled simulations

The tomography reconstruction is also available for radial profiles at different axial positions, so a more detailed comparison between this two simulations was made in Fig. 12. Three computed and reconstructed liquid volume fraction radial profiles are compared. The axial locations are the same as in the case of projected mass density analyses ($x = 0.1$ mm, 2 mm and 6 mm downstream of the nozzle exit). The radial dispersion at all locations is seen to be quite similar for both simulations. However, remarkable differences for the top-hat profile case can be observed in terms of the peak value, in

agreement with Fig. 11 (right). Largest discrepancies appear at 6 mm and further downstream in comparison with the ones previously seen in terms of projected mass density in Fig. 9, accounting for the effects of the internal nozzle flow in the near nozzle region of the spray.

All these results, concerning the internal nozzle flow simulation effects in the developing of the first millimeters of the spray can be also seen in terms of velocity. In Fig. 13, the axial velocity at three different locations for both CFD simulations is shown. The simulation using the internal nozzle flow outlet profiles predicts a higher axial velocity in the near-field, which progressively decays till matching the predictions of the top-hat profile simulations from 6 mm downstream. This result indicates that the effects of the nozzle exit profiles obtained with a coupled simulation, have some impact only in the near-field region, while predictions for the far-field are almost the same as the ones made by a simulation with a flat inlet radial profile.

To sum up this final study, a lower accuracy in the near region (i.e., within 10 mm) is achieved by the simulations without the nozzle geometry, although agreement is still quite remarkable with the experimental measurements in the case of the projected density, as shown in previous works [9]. Nevertheless, the effects of the internal nozzle flow profile in the near region of the spray are shown in the liquid volume fraction radial profiles as well the radial profiles of axial velocity. The different velocity profile and the subsequent induced turbulent viscosity modifies spray dispersion and then liquid volume

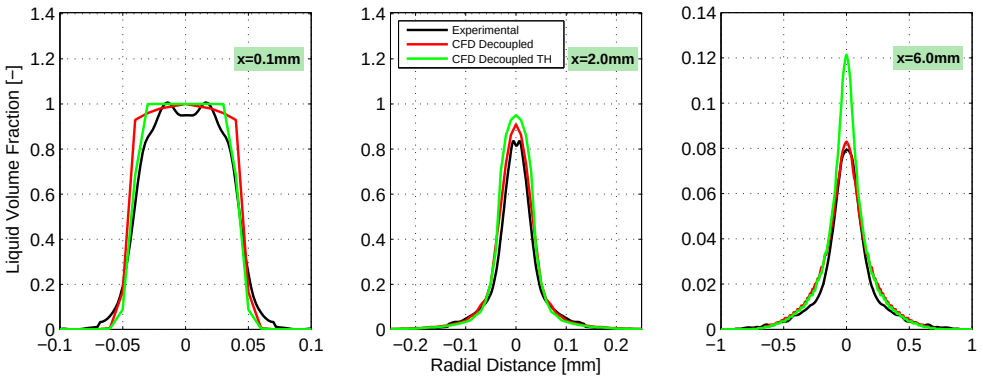

Figure 12: Computed and reconstructed liquid volume fraction radial profiles at 1 ms after SOI at axial locations of 0.1 mm, 2 mm, and 6 mm downstream of the nozzle exit for different types of 2D decoupled simulations

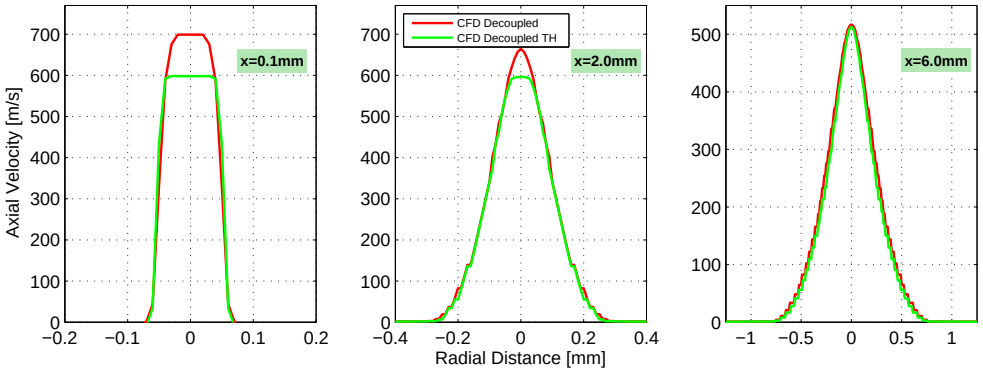

Figure 13: Computed radial profiles of axial velocity at 1 ms after SOI at axial locations of 0.1 mm, 2 mm, and 6 mm downstream of the nozzle exit for different types of 2D decoupled simulations

fraction profiles in the near nozzle region. Further downstream the profile shape effect vanishes, probably due to the fact that mass and momentum flux of both simulations is similar.

6. Summary and Conclusions

The Σ-Y Eulerian atomization model has been applied to the study of direct injection diesel sprays, with a focus on reproducing the internal structure of a diesel spray in the near-field, including the effects of internal nozzle flow. Calculations have been validated against x-ray radiography measurements of non-evaporating Spray A condition of ECN, conducted at Argonne National Laboratory. The present work is limited to a non-cavitating nozzle, but it has to be noticed that the trend in industry is towards highly tapered nozzles that are less prone to cavitation. So the conclusions may be applied to other nozzles used in Diesel injection systems.

First of all, a novel constraint on turbulent mixing driven multiphase flows has been derived and implemented. This constraint prevents the mixing velocity from exceeding the magnitude of the turbulent fluctuations. Although it does not have a significant influence on the spray development, it increases the stability of the model, which allows simulations to run at higher Courant numbers.

The main outcome of this paper is the study of the effect of including nozzle flow on diesel spray CFD simulations, using the Eulerian Σ-Y

atomization model. 3D and 2D coupled internal/external flow simulations were compared. Both calculations produced qualitatively and quantitatively good agreement with the experimental data, showing that 3D simulations can capture measured flow asymmetries close to the nozzle outlet, but 2-D simulations provides accurate results within a few diameters downstream. Additionally, in order to explore the necessity of the coupled simulation, two studies in a domain without the nozzle geometry were run. In one case, the inlet boundary condition is taken from the coupled simulation and in the other, a top-hat velocity profile, obtained from mass flow rate and momentum flux measurements, is applied at the nozzle outlet. Apart from the near-field study, the effect on further spray development (i.e. far field) was evaluated. These two simulations have been compared in terms of spray penetration and liquid volume fraction, detecting some influence of the internal nozzle flow profile in the first instants of the spray penetration. Also, a noticeable impact on the intact core length prediction and LVF profiles were reported. However, further downstream the differences vanishes and tip penetration and velocity field are nearly the same, indicating that injected mass and momentum flux plays a major role on spray turbulent mixing.

At the sight of the results, the Σ-Y Eulerian atomization model has proved its ability to model the internal flow together with the spray, providing fairly good predictions to match with the experimental data. A remarkable conclusion of the present contribution is that when a good measurement of rate of injection (ROI) is available, and the study involves a single-hole convergent nozzle, a two-dimensional eulerian study without the internal flow simulation is perhaps sufficient. Obviously, if the aim of the work is evaluating the effects of asymmetries of the nozzle geometry, a full 3D coupled simulation (internal nozzle and spray) will be the proper solution.

Acknowledgement

Authors acknowledge that part of this work was possible thanks to the Programa de Ayudas de Investigación y Desarrollo (PAID-2013 3198) of the Universitat Politècnica de València. Also this study was partially funded by the Spanish Ministry of Economy and Competitiveness in the frame of the COMEFF(TRA2014-59483-R) project.

References

[1] Beale, J. and Reitz, R., Modeling spray atomization with the kelvin-helmholtz/rayleigh-taylor hybrid model, *Atomization and Sprays*, vol. **9**, no. 6, pp. 623–650, 1999.

[2] Beau, P., Funk, M., Lebas, R., and Demoulin, F., Applying quasi-multiphase model to simulate atomization processes in diesel engines: Modeling of the slip velocity, *SAE Technical Paper 2005-01-0220*, 2005.

[3] Belhadef, A., Vallet, A., Amielh, M., and Anselmet, F., Pressure-swirl atomization: Modeling and experimental approaches, *International Journal of Multiphase Flow*, vol. **39**, pp. 13 – 20, 2012.

[4] Blokkeel, G., Barbeau, B., and Borghi, R., A 3D Eulerian model to improve the primary breakup of atomizing jet, *SAE Technical Paper 2003-01-005*, 2003.

[5] Çengel, Y. A. and Boles, M. A., *Thermodynamics: an engineering approach*, McGraw Hill Higher Education, 2011.

[6] Dahms, R. N., Manin, J., Pickett, L. M., and Oefelein, J. C., Understanding high-pressure gas-liquid interface phenomena in diesel engines, *Proceedings of the Combustion Institute*, vol. **34**, no. 1, pp. 1667 – 1675, 2013.

[7] Demoulin, F., Beau, P., Blokkeel, G., Mura, A., and Borghi, R., A new model for turbulent flows with large density fluctuations: application to liquid atomization, *Atomization and Sprays*, vol. **17**, pp. 315–345, 2007.

[8] Demoulin, F.-X., Reveillon, J., Duret, B., Bouali, Z., Desjonqueres, P., and Menard, T., Toward using direct numerical simulation to improve primary break-up modeling, *Atomization and Sprays*, vol. **23**, no. 11, pp. 957–980, 2013.

[9] Desantes, J., García, J., Pastor, J., and Pandal, A., A comparison of diesel sprays CFD modelling approaches: DDM vs $\Sigma - Y$ eulerian atomization model, *Atomization and Sprays*, 2016 (accepted).

[10] Desantes, J., Payri, R., Garcia, J., and Salvador, F., A contribution to the understanding of isothermal diesel spray dynamics, *Fuel*, vol. **86**, no. 78, pp. 1093 – 1101, 2007.

[11] Desportes, A., Zellat, M., Desoutter, G., Liang, Y., and Ravet, F., Application of the Eulerian-Lagrangian spray atomization (ELSA) model for the diesel injection simulation, *THIESEL 2010 Conference on Thermo- and Fluid Dynamic Process in Diesel Engines*, 2010.

[12] Dukowicz, J., A particle fluid numerical model for liquid sprays, *Journal of Computational Physics*, vol. **2**, pp. 111–566, 1980.

[13] ECN, Engine combustion network, 2nd workshop proceedings of sessions: 'Mixing and Velocity' and 'Spray Development and Vaporization', 2012.
URL `http://www.sandia.gov/ecn/workshop/ECN2.php`

[14] ECN, Engine combustion network data archive, 2012.
URL `http://www.sandia.gov/ecn/`

[15] ECN, LVF data archive, 2014.
URL `http://www.sandia.gov/ecn/argonne/assets/datafiles/mixture/rad675.php`

[16] García-Oliver, J., Pastor, J., Pandal, A., Trask, N., Baldwin, E., and Schmidt, D., Diesel spray CFD simulations based on the $\Sigma - Y$ eulerian atomization model, *Atomization and Sprays*, vol. **23**, pp. 71–95, 2013.

[17] Kastengren, A., Tilocco, F. Z., Powell, C. F., Manin, J., Pickett, L. M., Payri, R., and Bazyn, T., Engine combustion network (ECN):measurements of nozzle geometry and hydraulic behavior, *Atomization and Sprays*, vol. **22**, pp. 1011–1052, 2012.

[18] Kastengren, A. L., Powell, C. F., Wang, Y., Im, K.-S., and Wang, J., X-ray radiography measurements of diesel spray structure at engine-like ambient density, *Atomization and Sprays*, vol. **19**, no. 11, pp. 1031–1044, 2009.

[19] Kastengren, A. L., Tilocco, F. Z., Duke, D. J., Powell, C. F., Seoksu, M., and Xusheng, Z., Time-resolved x-ray radiography of diesel injectors from the engine combustion network, *ICLASS Paper*, no. 1369, 2012.

[20] Lebas, R., Menard, T., Beau, P., Berlemont, A., and Demoulin, F., Numerical simulation of primary break-up and atomization: DNS and modeling study, *International Journal of Multiphase Flow*, vol. **35**, pp. 247–260, 2009.

[21] Lee, C. H. and Reitz, R. D., {CFD} simulations of diesel spray tip penetration with multiple injections and with engine compression ratios up to 100:1, *Fuel*, vol. **111**, no. 0, pp. 289 – 297, 2013.

[22] Lucchini, T., D'Ericco, G., and Ettorre, D., Numerical investigation of the spray-mesh-turbulence interactions for high-pressure, evaporating sprays at engine conditions, *International Journal of Heat and Fluid Flow*, vol. **32**, pp. 285–297, 2011.

[23] Macián, V., Bermúdez, V., Payri, R., and Gimeno, J., New technique for determination of internal geometry of a diesel nozzles with the use of silicone methodology, *Experimental Techniques*, vol. **37**, pp. 39–43, 2003.

[24] Martí-Aldaraví, P., Development of a computational model for a simultaneous simulation of internal flow and spray break-up of the Diesel injection process, PhD thesis, Departamento de Máquinas y Motores Térmicos, Universidad Politécnica de Valencia, España, 2014.

[25] Naber, J. and Siebers, D., Effects of gas density and vaporization on penetration and dispersion of diesel sprays, *SAE Technical Paper*, no. 960034, 1996.

[26] Ning, W., Reitz, R., Diwakar, R., and Lippert, A., An Eulerian-Lagrangian spray and atomization model with improved turbulence modeling, *Atomization and Sprays*, vol. **19**, pp. 727,739, 2009.

[27] Payri, R., García, J., Salvador, F., and Gimeno, J., Using spray momentum flux measurements to understand the influence of diesel nozzle geometry on spray characteristics, *Fuel*, vol. **84**, no. 5, pp. 551 – 561, 2005.

[28] Payri, R., Salvador, F., Gimeno, J., and de la Morena, J., Effects of nozzle geometry on direct injection diesel engine combustion process, *Applied Thermal Engineering*, vol. **29**, no. 10, pp. 2051 – 2060, 2009.

[29] Pickett, L., Manin, J., Kastengren, A., and Powell, C., Comparison of near-field structure and growth of a diesel spray using light-based optical microscopy and x-ray radiography, *SAE Int. J. Engines*, vol. **7**, no. 2, 2014.

[30] Pope, S., An explanation of the turbulent round-jet/plane-jet anomaly, *AIAA*, vol. **16**, pp. 279–281, 1978.

[31] Reid, R., Prausnitz, J., and Poling, B., *The Properties of Gases and Liquids*, McGraw-Hill, 1987.

[32] Salvador, F., Gimeno, J., Pastor, J., and Martí-Aldaraví, P., Effect of turbulence model and inlet boundary condition on the diesel spray behavior simulated by an eulerian spray atomization (ESA) model, *International Journal of Multiphase Flow*, vol. **65**, pp. 108–116, 2014.

[33] Siebers, D., Liquid-phase fuel penetration in diesel sprays, *Trans. SAE*, vol. **107**, pp. 1205–1227, 1998.

[34] Siebers, D., Liquid-phase fuel penetration in diesel sprays based on mixing-limited vaporization, *Trans. SAE*, vol. **108**, pp. 703–728, 1999.

[35] Siebers, D. L., 2008. Recent developments on diesel fuel jets under quiescent conditions, *Flow and combustion in reciprocating engines*. Arcoumanis, C. and Kamimoto, T. (Eds.). Springer-Verlag, Berlin, pp. 257–308.

[36] Som, S., Longman, D., Ramrez, A., and Aggarwal, S., A comparison of injector flow and spray characteristics of biodiesel with petrodiesel, *Fuel*, vol. **89**, no. 12, pp. 4014 – 4024, 2010.

[37] Som, S., Ramirez, A. I., Longman, D. E., and Aggarwal, S. K., Effect of nozzle orifice geometry on spray, combustion, and emission characteristics under diesel engine conditions, *Fuel*, vol. **90**, no. 3, pp. 1267 – 1276, 2011.

[38] Trask, N., Schmidt, D., Lightfoot, M., and Danczyk, S., Compressible modeling of the internal flow in a gas-centered swirl-coaxial fuel injector, *Journal of Propulsion and Power*, vol. **28(4)**, pp. 685–693, 2012.

[39] Vallet, A. and Borghi, R., Modélisation Eulerienne de l'atomisation d'un jet liquide, *C.R. Acad. Sci, Paris*, vol. **327**, pp. 1015–1020, 1999.

[40] Vallet, A., Burluka, A., and Borghi, R., Development of a Eulerian model for the "atomization" of a liquid jet, *Atomization and Sprays*, vol. **11**, pp. 619–642, 2001.

[41] Wang, Y., Lee, W., Reitz, R., and Diwakar, R., Numerical simulation of diesel sprays using an eulerian-lagrangian spray and atomization (ELSA) model coupled with nozzle flow, *SAE Technical Paper 2011-01-0386*, 2011.

[42] Weller, H., Tabor, G., Jasak, H., and Fureby, C., A tensorial approach to computational continuum mechanics using object-oriented techniques, *Computers in Physics*, vol. **12**, pp. 620–631, 1998.

[43] Xue, Q., Battistoni, M., Powell, C., Longman, D., Quan, S., Pomraning, E., Senecal, P., Schmidt, D., and Som, S., An eulerian CFD model and x-ray radiography for coupled nozzle flow and spray in internal combustion engines, *International Journal of Multiphase Flow*, vol. **70**, no. 0, pp. 77 – 88, 2015.

[44] Xue, Q., Battistoni, M., Som, S., Quan, S., Senecal, P. K., Pomraning, E., and Schmidt, D. P., Eulerian cfd modeling of coupled nozzle flow and spray with validation against x-ray radiography data, *SAE Int. J. Engines*, vol. **7(2)**, pp. 1061–1072, 2014.

[45] Xue, Q., Som, S., Senecal, P. K., and Pomraning, E., Large eddy simulation of fuel-spray under non-reacting ic engine conditions, *Atomization and Sprays*, vol. **23**, no. 10, pp. 925–955, 2013.